Modelling of transport properties of graphene field-effect transistor for sensor application

Geoffrey Ijeomah* and Fahmi Samsuri

Faculty of Electrical and Electronics Engineering,
Universiti Malaysia Pahang,
26600 UMP Pekan, Pahang, Malaysia
Email: guijeomah2@gmail.com
Email: fahmi@ump.edu.my
*Corresponding author

Mohamad Adzhar Md Zawawi

School of Electrical and Electronic Engineering,
Universiti Sains Malaysia,
14300 Nibong Tebal, Penang, Malaysia
Email: adzhar@usm.my

Abstract: A dual-gated ultra-thin graphene field effect transistor (GFET) suitable for electronic sensing application is modelled. The applied simulation approach reproduces accurately the transport properties of the GFET characteristics and enables investigation of the influence of the different physical, biological and chemical factors. The simulation readouts and additional charges in the system are interpreted in the form of current-voltage characteristics and shift in Dirac peaks. These features could be extracted to predict the sensing mechanism of the GFET.

Keywords: graphene; graphene field effect transistor; GFET; sensor; current-voltage characteristics.

Reference to this paper should be made as follows: Ijeomah, G., Samsuri, F. and Zawawi, M.A.M. (2020) ‘Modelling of transport properties of graphene field-effect transistor for sensor application’, *Int. J. Biomedical Nanoscience and Nanotechnology*, Vol. 4, Nos. 1/2, pp.105–119.

Biographical notes: Geoffrey Ijeomah received his BEng degree in Electrical/Electronic Engineering from the Federal University of Technology, Owerri, Nigeria in 2009. He received his MEng degree in Electrical-Electronics and Telecommunication from Universiti Teknologi Malaysia in 2015. He is currently pursuing his doctorate degree (PhD) at Universiti Malaysia Pahang (UMP). He has research interests in electron transport in low dimensional nanostructures, nanofabrication, nanoscale sensor design and biomedical nanotechnology.

Fahmi Samsuri received his BEng (Hons) in Electrical, Electronics and System Engineering from Universiti Kebangsaan Malaysia (UKM) Bangi, Malaysia in 1999. He received his Masters degree in Electrical, Electronics and System Engineering from Universiti Kebangsaan Malaysia (UKM) Bangi, Malaysia in 2002. He received his PhD in Electrical and Computer Engineering from University of Canterbury, Christchurch, New Zealand in 2011. He is currently

Copyright © 2020 Inderscience Enterprises Ltd.

an Associate Professor at the Faculty of Electrical and Electronics Engineering, Universiti Malaysia Pahang (UMP) and a member of the Applied Electronics and Computer Engineering Group. His research interests are in microelectronics, nanofabrication, biochip design & fabrication, bio-nano materials, radio frequency (RF) and wireless communication.

Mohamad Adzhar Md Zawawi received his BEng degree in Electrical and Electronic Engineering from the University of Sheffield in 2003. He received his MSc degree in Electronic Systems Design Engineering from Universiti Sains Malaysia in 2010 and PhD in Electrical and Electronic Engineering from the University of Manchester in 2015. He currently holds an academic position within the School of Electrical and Electronic Engineering, USM. His research interests are in the field of micro/nanoelectronics fabrication, modelling and simulation of nano devices and sub-Thz and Thz MMIC oscillator based on resonant tunnelling diodes.

1 Introduction

Graphene is a two-dimensional (2-D), sp^2 hybridised allotrope of carbon with sheets of carbon atoms cascaded in honeycomb lattice structure. Due to its promising properties, such as superior electrical conductivity, high thermal conductivity, high carrier mobility, large surface-to-volume ratio and good optical properties, graphene can be considered as an attractive platform for electronic sensing application. Moreover, graphene is believed to promote virtually unlimited design possibilities of sensors that are ultra-selective, more sensitive, faster, compact, inexpensive and smaller compared to traditional sensors. The majority of reported graphene-based sensor devices exploit a field effect transistor device with graphene as the channel electrode as shown in Figure 1.

Figure 1 Schematic of graphene field effect transistor sensor circuit (see online version for colours)

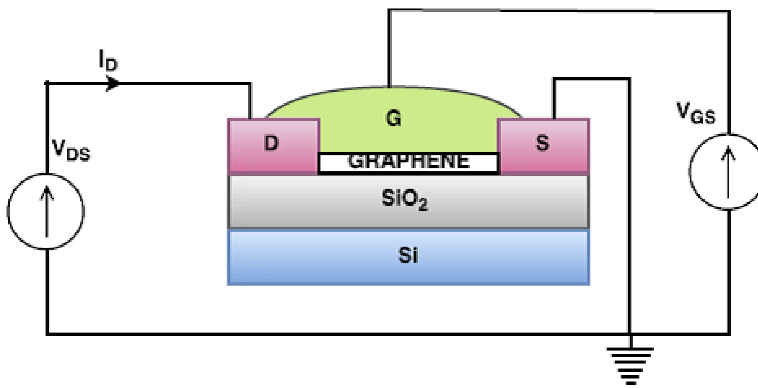

Generally, the field effect transistor consists of three electrodes – source (S), drain (D) and the gate insulator (G), and is therefore comparable in operation to the conventional metal oxide semiconductor field effect transistor (MOSFET). The principle of operation of FET is based on the field effect promoting the conductance of the semiconducting

element in the channel region via the applied field bias generated by the external chemical potential. In particular, the flow of carriers from the source electrode to the drain electrode is modulated by the applied electric field across the source and the insulated gate. Thus, in a typical MOSFET, the drain current I_D is a function of the electric field applied, V_{GS} across the source and gate terminals (Balogh, 2017; Chang et al., 2017; Monga et al., 2010).

The field effect technology is still evolving with recent research work focusing on either improving the existing FET parameters or scaling down the devices (Dasgupta, 2007; Gili et al., 2004). Nevertheless, the relentless research interest in graphene-based transistors would confirm the suspicion that GFETs can compete with the conventional MOSFET technology which has been the technology of interest for decades. Previous GFET devices utilised a 300 nm SiO_2 insulating dielectric layer and a highly doped Si substrate as a back-gate. Such technologies, however, encountered unseemly large parasitic capacitances and could not be coupled to other technologies. To overcome this limitation, practical GFET devices have been designed to incorporate a top-gate electrode (Ijeomah, 2018). It should be noted that the unique geometry of graphene and the presence of high carrier mobility make graphene a promising candidate for varying FET applications (Viswanathan et al., 2015; Varghese et al., 2015), particularly in the field of sensing and detection of various physical, biological and chemical analytes.

The prediction of the properties of a new-fangled design is always a critical issue during the development phase because the realisation of a prototype (particularly in the case of a transistor) may be perhaps challenging due to the requirement of specialised equipment and convoluted technological processes. This is why the simulation approach is the most viable option to bypass these challenges. The goal of this work is to investigate the performance characteristics of a modelled graphene field effect transistor (GFET) that can used in sensor application.

2 Theory

Graphene is a zero bandgap, low-dimensional material with a linear dispersion relation near the Fermi level. It has been demonstrated during various instrumentations that large-area-graphene field effect transistors manifest distinctive current-voltage (I-V) characteristics. The carrier density and the nature of carriers in the channel are correlated to the differential in the applied electric field across the insulting gate and the channel. As expected, positive applied bias results in an n-type carrier whereas negative applied bias promotes p-type carrier within the channel. The result is the appearance of the so called charge neutrality point on the I-V characteristics of the device. At the charge neutrality point, the maximum resistance and minimum conductivity are prominent. The magnitude of the current at the charge neutrality point depends on such factors as the doping level of graphene sheet, nature of the charges residing at the bottom and top of the channel, quality of the substrate and the type of electric contacts. Of all these features, the doping concentration is the most critical in the context of sensor application because numerous external factors such as ions or absorbed molecules could be considered as dopants which are responsible for the voltage shift at the charge neutrality point (Inaba et al., 2014). Therefore, for a charge neutrality point at the positive (or negative) applied voltage on the *I-V* characteristics, graphene is doped with holes (or electrons).

Now, let us consider a top-gate configuration of graphene field effect transistor in the quantum capacitance limit regime (see Figure 2), where the quantum capacitance is much less than the gate capacitance, $C_q \ll C_G$. We further examine this model since it is able to elicit the salient features of graphene field effect transistors. In the quantum capacitance regime, the drain current I_D is given by (Ariel, 2012),

$$I_D = \frac{eW}{L}\int_0^L n(x)v_d\,dx \tag{1}$$

where L is the channel length, W is the width of the gate channel and x is the position along the channel. Thus, the drift velocity v_d can now be expressed as,

$$v_d = \mu E \Big/ \left[1+\left(\mu E/v_{sat}\right)^{\alpha}\right]^{1/\alpha} \tag{2}$$

where v_{sat} is the saturation velocity that is invariant, μ is graphene mobility and $\alpha = 2$ for graphene-based transistors.

Figure 2 Schematic illustration of GFET (see online version for colours)

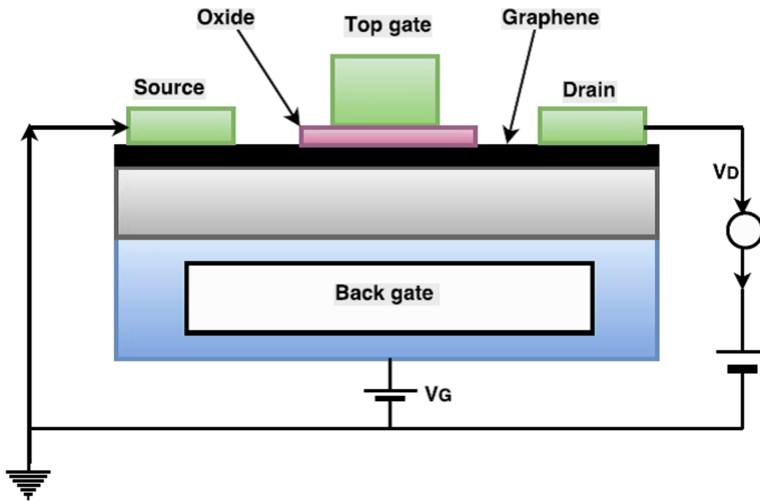

Note: The oxide substrate is made of SiO.

For a channel with length L proportional to the position x, the resulting channel voltage is given by,

$$V_{ch} = (X/L)V_D \tag{3}$$

Similarly, the resulting surface potential is given by,

$$\varphi_s(x) = V_G - V_{ch}(x) \tag{4}$$

Considering that,

$$n = n_0 + \left[e\varphi_s(x)\right]^2 \Big/ \pi\hbar v_F^2 \tag{5}$$

where n is the intrinsic charge carriers and n_0 is the concentration of impurities, we obtain the following models for the foremost DC characteristics $I_D = (V_D, V_G)$ of the GFET,

$$I_D\left(V_D, V_G\right) = e(W/L)\mu^* V_D\left[n_0 + \gamma\left(V_G^2 + V_D^2/3 - V_D V_G\right)\right] \tag{6}$$

where $\mu^* = \mu[1 + (\mu V_D/v_{sat}L)]$, $\gamma = e^2/\pi\hbar v_F^2$ is a constant and $n_0 \cong 10^{11}$ cm^{-2}.

On the other hand, if the channel mobility μ is not known, we can predict it from the DC measurement of $I_D(V_D, V_G)$ according to,

$$\mu = \frac{1}{en}\frac{\partial I_D/W}{\partial V_d/L} \tag{7}$$

The drain current-drain voltage I_D-V_D characteristics manifest three distinctive regions of operations as shown in Figure 3(a). The sublinear region (I) arises from the absence of bandgap in the graphene channel. The superlinear regime (II) reflects a super-extended ohmic region where the familiar Ohm's law no longer follows the linear current-voltage relation. The current saturates to a finite magnitude I_{sat} in the saturation regime (III) and the charge neutrality point is recovered at $V_D = V_G$.

Figure 3 (a) Drain current versus drain voltage curve showing sublinear (I), superlinear (II) and saturation (III) regions (b) Drain voltage versus gate voltage interdependency curve

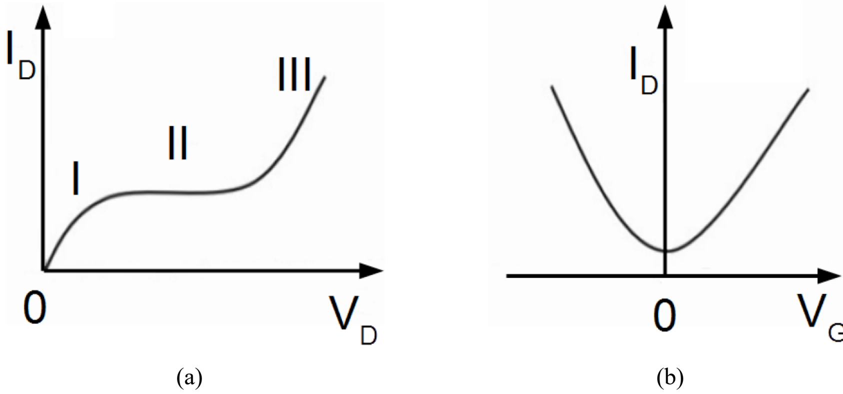

(a) (b)

The inter-dependence of the I_D-V_D characteristics is delineated in Figure 3(b). It should be noted that I_D does not vanish at $V_G = 0$ because of the minimum conductivity of graphene. The minimum value of the $I_D(V_G)$ characteristics occurs at the charge neutrality point. If the electric field at the charge neutrality point is less than V_G, an n-type conductivity results, and a p-type conductivity otherwise. As expected, the I_D-V_D characteristics exhibits an unusual 'V-like' formation for any GFET. The ambipolar transport, which is a signature characteristic of 2-D nanostructures, is at the centre of this V-shaped formation.

As previously established, the principle of operation of GFET is based on charge transport between the source and drain electrodes which can be tuned by the gate voltage. The correlation between the conductance and transmission probability of carrier transport conforms to Landauer formalism given by,

$$G = \frac{2q^2}{h}T \tag{8}$$

Applying the Taylor expansion series on the parabolic energy band structure of graphene (Ariel, 2012), we obtain,

$$E(k) \approx \frac{E_G}{2} + \frac{E_G}{4\beta^2} k_x^2 \tag{9}$$

where β is the quantised wave vector. The wave vector can then be extracted from the parabolic portion of the energy band as,

$$k = \sqrt{\frac{4E}{3a_{c-c}t} - 2\beta^2} \tag{10}$$

Based on this, we can now extract the conductance of the channel from equation (8) as,

$$G = \frac{6q^2}{hL} \sqrt{\left(a_{c-c} t\pi k_B T\right)} \left[\int_0^{+\infty} \frac{x^{-1/2}}{1 + e^{(x-\eta)}} + \int_0^{+\infty} \frac{x^{-1/2}}{1 _ e^{(x+\eta)}} \right] dx \tag{11}$$

where $x = (E - E_G)/k_BT$ and $\eta = (E_F - E_G)/k_BT$ is the normalised Fermi energy. Since the sensing mechanism of GFET can be predicted directly from its conductance or *I-V* characteristics, the corresponding current of the graphene channel can be expressed as,

$$I = \frac{6q^2}{hL} \left(a_{c-c} t\pi k_B T\right)^{1/2} \left[I_{-\frac{1}{2}} \left(\frac{E_F - \delta T - \lambda F}{k_B T} \right) + I_{-\frac{1}{2}} \left(\frac{\delta T + \lambda F - E_F}{k_B T} \right) \right] \left(V_{gs} - V_t\right) \tag{12}$$

3 Method

We know that the carrier transport in carbon nanotubes is not always in equilibrium due to the rapidly fluctuating built-in and external electric fields. In order to account for the non-equilibrium behaviour of the charge transport in carbon nanotubes, we need to completely solve the Boltzmann transport equation (BTE). Although the Monte Carlo simulation method has been a model of choice for the solution of the BTE in semiconductor devices (Hong and Jang, 2017; Hong, 2017), several authors have reported a direct solution of the BTE that enables a noise-free resolution of the carrier distribution function (Guo and Wang, 2017). This work exploits a straight-forward approach to compute $f(x, v)$ for carbon nanotubes by solving the steady-state BTE self-consistently with the Poisson solver. We solve the BTE strictly in velocity and position, and consider the carrier transport within the relaxation time approximation, where individual scattering processes are depicted with a characteristic scattering rate that can be predicted from quantum mechanical principles.

The BTE describes the carrier transport dynamics of the semi-classical distribution function, $f(r, v, t)$ under the effect of non-identical scattering processes, as well as electric and magnetic fields. Neglecting the magnetic field contribution, the steady-state, space-phase BTE for $f(x, v)$ can be expressed as,

$$-\frac{eE(x)}{m^*} \frac{\partial f}{\partial v} + v \frac{\partial f}{\partial x} = \frac{f - fLE(x, v)}{\tau(\varepsilon)} \tag{13}$$

where $f_{LE}(x, v)$ is the local equilibrium distribution function appropriate to the applied bias, density and equilibrium lattice temperature T_0, to which $f(x, v)$ relaxes at a relaxation rate $\tau(\varepsilon)^{-1}$. We also choose the Maxwell-Boltzmann distribution at T_0 appropriate to normalise the local density as $n(x)$,

$$f_{LE}(x, v) = n(x)\left[\frac{m^*}{2\pi kT_0}\right]^{\frac{1}{2}} \cdot e^{\frac{m^* v^2}{2k_B T_0}} \tag{14}$$

The non-identical electric field $E(x)$ in the Boltzmann transport equation arising from the spatially dependent doping and carrier densities, $N_D(x)$ and $n(x)$ is extracted from the Poisson equation,

$$\frac{d^2\phi}{dx^2} = -\frac{dE}{dx} = -e\frac{N_D(x) - n(x)}{\in\in_0} - \rho(x) \tag{15}$$

where e is the non-dynamic dielectric constant. Since the electron density and the distribution function are correlated by,

$$n(x) = \int_{-\infty}^{+\infty} f(x, v)dv \tag{16}$$

The Boltzmann and Poisson equations form a nonlinear, coupled set of equations, requiring equations (13)–(16) to be solved self-consistently.

Figure 4 General model of the coaxially gated graphene (applicable to carbon nanotubes) field effect transistor with semi-infinite, heavily doped channel as the source/drain contacts (see online version for colours)

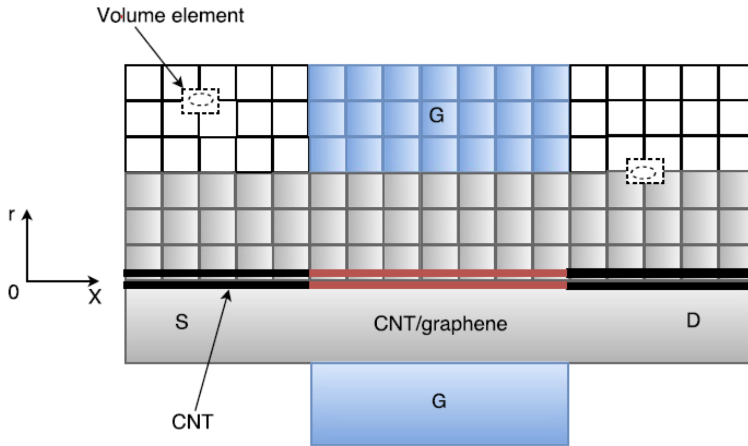

Notes: Also shown are the simulation grid, simulated area and a volume element assumed to be in cylindrical coordinate arrangement used for solving the Poisson equation. The dashed rectangular structure delineates the element adopted to linearise the Poisson equation at position (x_i, r_j).

The simulation technique is performed self-consistently with Poisson equation. Figure 4 depicts the model of the GFET that yields the theoretical best control over the graphene channel. The source and drain electrodes are heavily doped and the gate

electrode modulates the conductance of the channel, akin to the conventional MOSFET. For the model of Figure 4, we employed the self-energies described in Svensson and Campbell (2011), which makes our method perfectly applicable to one-dimensional (1-D) carbon nanotubes.

As the current-voltage characteristics of the GFET device is dependent on both the carrier transport and the electrostatic potential, we implemented a self-consistent iteration between the Boltzmann transport equation and Poisson equation. The procedure is as follows: for a given carrier density, the Poisson equation is solved to obtain the potential profile in the graphene channel. Next, the computed potential profile is exploited as the input to the BTE, and an improved guess is obtained. The iteration process between the BTE and Poisson equation is repeated until a self-consistent profile is obtained. Finally, the current for the self-consistent scheme is computed.

For the model of Figure 4, it is appropriate to solve the Poisson equation in cylindrical coordinates. Since the potential and carrier density are invariant around the GFET channel, the Poisson equation is basically a two-dimensional (2-D) problem in the x-direction (channel direction) and r-direction (radial to the channel) as indicated in Figure 4. Within this boundary condition, the Poisson equation can be expressed as,

$$\Delta^2 E_m(r, z) = -\frac{e}{\varepsilon}\rho \tag{17}$$

where E_m is the energy state devoid of the work function of the channel, and it is indeed the mid-point energy for the grid points on the channel surface, ρ is the carrier density, which could be relaxed to zero for grids outside the surface of the channel and non-zero otherwise. The electric field is relaxed to zero at $r = 0$ (Auth and Plummer, 1997), thus,

$$\varepsilon_r\big|_{r=0} = 0 \tag{18}$$

Since we can predict the potential at the gate electrode, exploiting the Fermi level of the grounded channel as the zero energy will result in a gate electrode potential equal to,

$$E_m(gate) = -eV_G + \phi_{ms} \tag{19}$$

where V_G is the applied gate bias and ϕ_{ms} is the variation in the work function between the gate electrode and the channel. By simulating a sizeable area (see Figure 4), the remaining boundaries can be subjected to the Neumann boundary conditions where the applied bias perpendicular to the boundary is taken to be zero.

The continuous form of equation (17) is then discretised for computer simulation. It is appropriate to take a volume element close to the grid point (see Figure 4) and subject it to the integral form of the Poisson equation, which is a ring around the channel axis with a rectangular cross section,

$$\int \vec{D}\cdot d\vec{S} = q_{ij} \tag{20}$$

where q_{ij} denotes the charge in the overall volume element. The discretised equation for an element suspended on the grid point (x_i, r_j) in space is,

$$er_j\Delta\left(N_D - n_{net}\right) = \varepsilon_0\left(\frac{r_{j-1}+r_j}{2}\Delta x\frac{E_m^{i,j-1}-E_m^{i,j}}{\Delta r}+\frac{r_{j+1}+r_j}{2}\Delta x\frac{E_m^{i,j}}{\Delta r}\right) + r_j\Delta r\frac{E_m^{i+1,j}-E_m^{i,j}}{\Delta x}+r_j\Delta r\frac{E_m^{i-1,j}-E_m^{i,j}}{\Delta x} \quad (21)$$

For grid points located in the gate insulator, the dielectric of the gate insulator replaces the ε_0 term in equation (21). For the grid points located at the space-gate insulator interface, the space dielectric is used for the volume surfaces in space and the gate dielectric is used for the volume surfaces in the gate insulator.

Equation (21) is linear and computationally easy to solve, but the convergence of the linear Poisson equation and carrier transport is poor. A nonlinear Poisson equation, which associates the potential through a nonlinear dummy function to the carrier density has been shown to be particularly promising in improving the convergence of the BTE-Poisson loop. The nonlinear dummy function correlating the potential and carrier density should be close to the physical correlation provided by the carrier transport equation as possible for improved convergence. In most cases, a semi-classical, equilibrium carrier statistics with a dummy quasi-Fermi level is employed as the dummy function. Then the nonlinear Poisson equation is solved for its potential profile using Gummel iteration method. Details of the nonlinear Poisson solver can be found here (Uysal and Tanoglu, 2017; Xie, 2017).

4 Results and discussion

Figure 5 shows the drain-source current versus drain-source voltage (I_{DS}-V_{DS}) of the graphene field effect transistor. The top gate spans a voltage of 8–14 volts. It is clear that the electric field across the drain channel is not substantial enough to allow current saturation in the device. This is in direct contrast to carbon nanotube-based field effect transistors (GFETs) where high applied bias drives the current to saturate to a saturation value of I_{sat}. This makes graphene a preferred and promising alternative to carbon nanotubes in sensor applications. This is because the presence of current (or voltage) saturation significantly affects the carrier transport within the device and hence the fundamental laws governing sensor circuit design and applications. Due to the ultra-thin nature of the modelled GFET, the applied voltage across the drain terminal was not increased above 0.2 V threshold in order to circumvent device cracking. To attain current (or voltage) saturation, therefore, the transport carriers would need to advance in the same direction in graphene. This latter action requires a driving potential that is greater than the Fermi energy (although electron-electron scattering may make this almost impossible), as well as reducing the ultra-thin nature of graphene through careful simulation. However, this would mean increased sample size which will ultimately increase computation space and time.

Figure 5 The drain-source current versus drain-source voltage of graphene (see online version for colours)

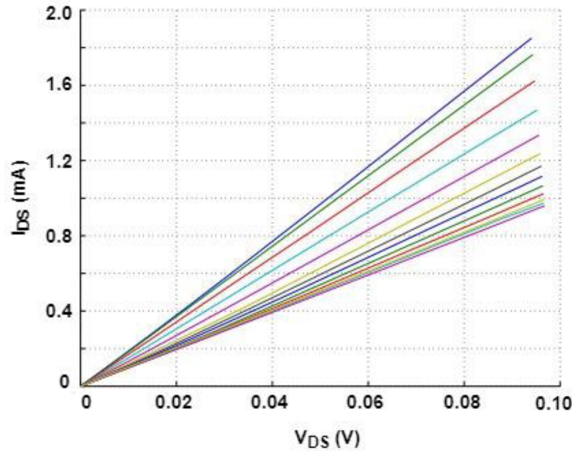

Notes: The top gate is varied from 8–14 V with 0.5 step size. The back gate voltage is assumed to be zero for simplicity.

Figure 6 shows the output characteristics of the modelled graphene field effect transistor which is comparable to the current-voltage (*I*-*V*) characteristics of a typical field effect transistor characteristics. The linear and saturation regions are conspicuous particularly for applied voltages much less than the Dirac voltage. The saturation current at the drain terminal I_{Dsat} is now a function of the gate-source voltage which is a signature feature of field effect transistors. However, there are also apparent discrepancies between the conventional field effect transistors and graphene-based field effect transistors as captured in Figure 7. It is obvious from Figure 7 that the I_D-V_{GS} output characteristics of the GFET differ from those of a typical MOSFET. Here, the voltage limit $V_{GS(\text{lim})}$ is not apparent so the GFET is in a conduction state in all the regime of V_{GS} voltage. The drain current I_D drives towards its minimum value for V_{GS} contiguous to the charge neutrality point voltage employed in the program set-up for device simulation. One can also observe a slight shift of the charge neutrality point voltage in the output characteristics which corresponds to the point of minimum conductance, towards positive magnitudes with increasing drain bias. This can be attributed to the influence of the drain bias on the channel potential (Song et al., 2016; Luszczek et al., 2017; Manoharan et al., 2017).

It should be pointed out, however, that charge conduction in GFET is ambipolar, that is, manifests an electron character for gate-source voltages greater than charge neutrality point voltage and a hole character for gate-source voltages less than the charge neutrality point voltage. It implies that GFET manifests, to a reasonable degree, features comparable to the n-FET for gate-source voltages greater than the charge neutrality point voltage. Nevertheless, I_D rises with decreasing gate-source voltages, although unlike the p-FET, it maintains same current trajectory as the n-FET.

Figure 6 The I_D versus V_{DS} output characteristics of the modelled graphene field effect transistor (see online version for colours)

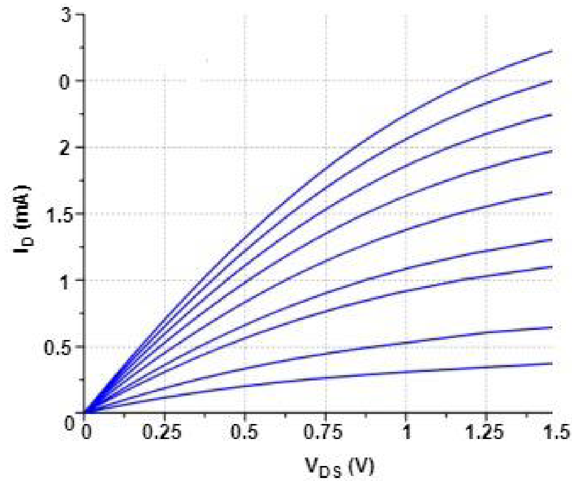

Figure 7 The $I_D - V_{GS}$ output characteristics of the modelled graphene field effect transistor for V_{DS} = 0.5 V, 1.0 V and 1.5 V respectively (see online version for colours)

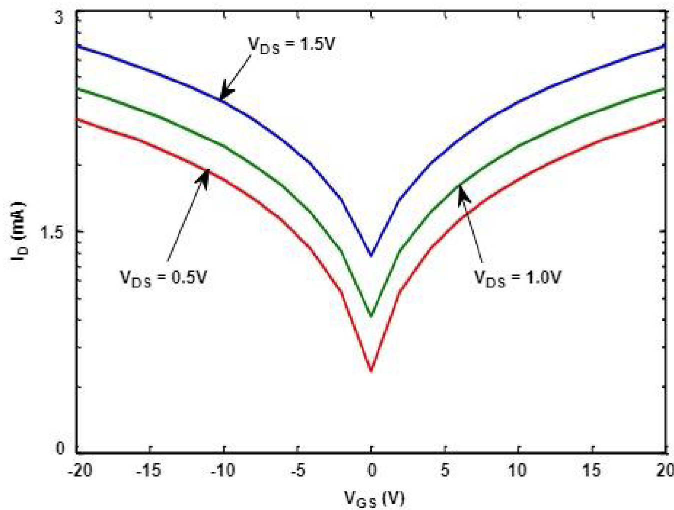

Figure 8 is the current-voltage (*I-V*) characteristics of the GFET when exposed to a selected target or analyte – an ammonia gas molecule (NH_3). Also shown is the experimental data (Ijeomah, 2018). Our model is in reasonable agreement with the experiment except the slight tilt towards the positive gate voltage at the charge neutrality point. This can be attributed to the carrier transport in the GFET which plays unique role in the sensing of the NH_3 gas molecules. This is as a result of the interaction of gas analyte molecules with graphene surface which causes carriers to traverse the surface of the graphene channel. The simulation is carried out at a constant NH_3 analyte concentration of 500 ppm over a temperature scale of (25–150)°C. The applied bias is found to exhibit slight sensitivity at lower operating temperatures only for small values of

the current. This can be attributed to the reluctance of the analyte gas molecules to be absorbed on the graphene surface at such operating temperatures. This means that analyte gas molecules lack sufficient transport motion to be contacted by the graphene channel, suggesting the presence of quasi-ballistic transport in the channel. For all temperature scales, the current was found to increase progressively. However, extremely high temperatures appear to drive the gate voltage to a negative value as indicated in Figure 8(d). This is because, as a reducing agent, NH_3 supplies negatively charged carriers to the channel, and in return becomes oxidised. As a result, the graphene Fermi level stretches towards its conduction band edges leading to a more negative gate voltage.

Figure 8 Current-voltage characteristics of CNT and graphene after exposure to 500 ppm of NH_3 at (a) 25, (b) 50, (c) 100 and (d) 150°C (see online version for colours)

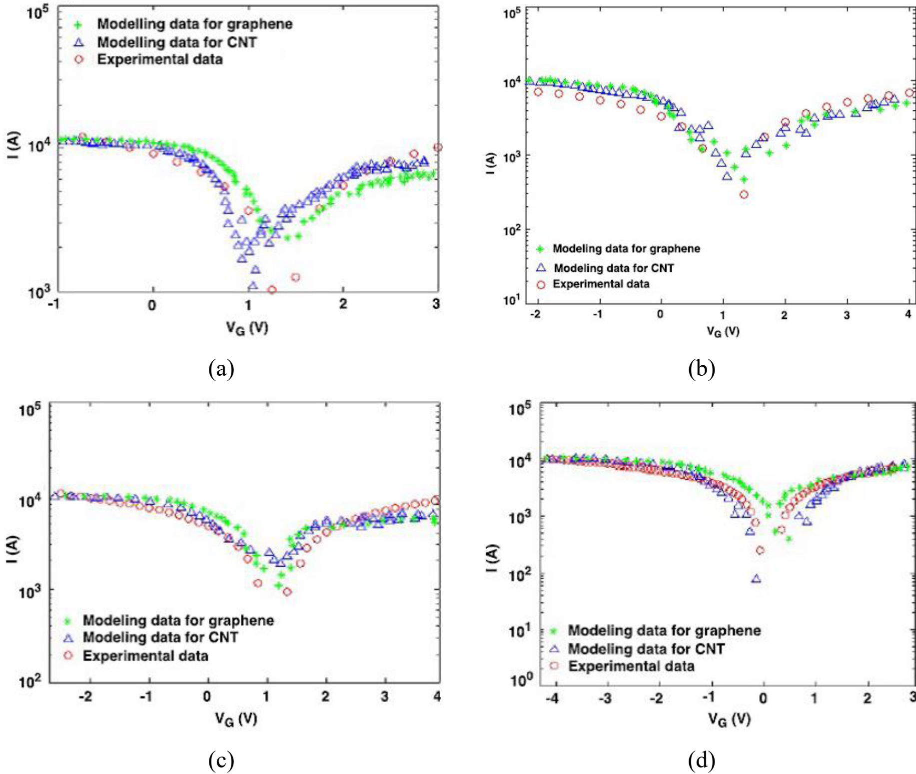

The developed models were also simulated for different ppm concentrations of NH_3 analyte gas. We could not go below 6 ppm NH_3 concentration due to the limitation of our model. Figure 9 shows the time evolution of Dirac shift for the simulated ppm concentrations of NH_3 analyte. Figure 9 is a fit to the experimental data (Chen et al., 2010) by a single exponential function,

$$V_{shift} = V_{\infty} + V_1 \exp(-1/\tau) \tag{22}$$

where V_{∞} is the steady state of the charge neutrality peak, t is time and τ_1 is the time constant. When fitted to equation (22), the 100 ppm concentration of NH_3 agreed well with data with a 98.9% precision. When fitted with the 150 and 200 ppm concentrations

of NH_3, an agreement of 98.5% and 96.9% were obtained respectively. However, when fitted to a double exponential function,

$$V_{shift} = V_{\infty} + V_1 \exp(-1/\tau) + V_2 \exp(-1/\tau_2), \tag{23}$$

the fit agreed well within a 99.8%, 99.9%, and 99.98% precision for the 100, 150 and 200 ppm concentrations of NH_3 molecules respectively. This suggests the existence of two dissimilar adsorption modes for the adsorption of the NH_3 analyte molecules on the surface of graphene channel. The computed time constants are: $\tau_1 = 25.46 \pm 3.84$, 2.25 ± 0.17 and $\tau_2 = 4.02 \pm 0.97$, 25.83 ± 1.10, with the prefactors yielding, $V_1 = 25.67 \pm 3.84$, 15.43 ± 0.50 and $V_2 = 11.13 \pm 2.32$, 22.01 ± 0.30 for the 100 and 200 ppm concentrations of the analyte respectively. These findings reinforce two outstanding sensing attributes of graphene-based field effect transistors. First, it reinforces the existence of two different modes of analyte adsorption which increases with increasing analyte concentration. Second, the rate of NH_3 analyte adsorption in the first mode is proportional to the concentration of the analyte molecules. However, the physical implication of this requires further theoretical investigations.

Figure 9 Time evolution of Dirac shift for different ppm concentration of NH_3 flow (see online version for colours)

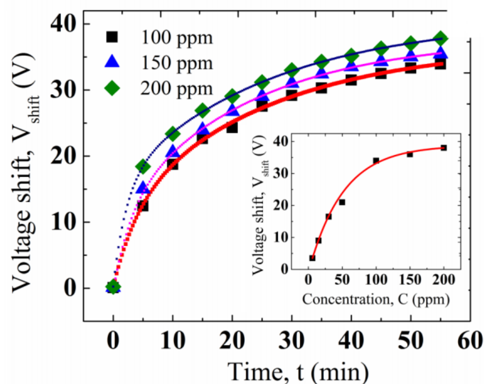

5 Conclusions

Since the first isolation of carbon-based electrodes, the understanding of graphene is evolving, and their role in field effect transistors is improving rather quickly. Behind this improvement is the underlying transport that arises due to the effect of electrochemical potential on the length scales of these devices. This work has employed simulation techniques to investigate the carrier transport properties of graphene, extracting the necessary parameters for electronic sensor application. The investigation showed distinct adsorption modes for the selected NH_3 analyte molecules which is indicative of the sensing mechanism of the device in real sensor application. The NH_3 analyte performed the role of a reducing agent as the charge neutrality point progressed towards the lower applied bias after the adsorption of analyte molecules.

References

Ariel, V. (2012) 'Energy band model based on effective mass', *Physics.gen-ph.*, Vol. 2, No. 1, pp.1–5.

Auth, C.P. and Plummer, J.D. (1997) 'Scaling theory for cylindrical, fully-depleted surrounding-gate MOSEFET's', *IEEE Electron Device Letters*, Vol. 18, No. 2, pp.74–76.

Balogh, L. (2017) *Fundamentals of MOSFET and IGBT Gate Driver Circuits*, Application Report SLUA618, Texas Instruments.

Chang, S-C., Avci, U.E., Nikonov, D.E. and Young, I.A. (2017) 'A thermodynamic perspective of negative-capacitance field-effect-transistors', *IEEE Journal on Exploratory Solid-State Computational Devices and Circuits*, Vol. 3, Vol. 2329, pp.56–64.

Chen, S., Cai, W., Chen, D., Ren, Y., Li, X., Zhu, Y. and Ruoff, R.S. (2010) 'Adsorption/desorption and electrically controlled flipping of ammonia molecules on graphene', *New Journal of Physics*, Vol. 12, No. 12, pp.1–8.

Dasgupta, A. (2007) 'Multiple gate MOSFETs: the road to the future', *International Workshop on Physics of Semiconductor Devices*, Vol. 7, pp.96–101.

Gili, E., Kunz, V.D., de Groot, C.H., Uchino, T., Ashburn, P., Donaghy, D.C., Hall, S., Wang, Y. and Hemment, P.L.F. (2004) 'Single, double and surround gate vertical MOSFETs with reduced parasitic capacitance', *Solid-State Electronics*, Vol. 48, No. 4, pp.511–519.

Guo, Y. and Wang, M. (2017) 'Heat transport in two-dimensional materials by directly solving the Boltzmann equation under Callaways dual relaxation model', *Physical Review B*, Vol. 96, No. 13, pp.1–17.

Hong, S-M. (2017) 'Transient simulation of graphene sheets using a deterministic Boltzmann equation solver', *Journal of Semiconductor Technology and Science*, Vol. 17, No. 2, pp.288–293.

Hong, S-M. and Jang, J-H. (2017) 'Transient simulation of semiconductor devices using a deterministic Boltzmann equation solver', *Electron Devices Society*, Vol. 6, No. 1, pp.156–163.

Ijeomah, G. (2018) *Theoretical Study of Transport Properties of Nanoscale Devices for Sensor Application*, PhD Dissertation, Universiti Malaysia Pahang, Malaysia.

Inaba, A., Yoo, K., Takei, Y., Matsumoto, K. and Shimoyama, I. (2014) 'Ammonia gas sensing using a graphene field-effect transistor gated by ionic liquid', *Sens. Actuators B Chem.*, Vol. 195, pp.15–21.

Luszczek, M., Swisulski, D., Hanus, R., Zych, M. and Petryka, L. (2017) 'Graphene field-effect transistor application for flow sensing', *EPJ Web of Conferences*, Vol. 143, pp.1–4.

Manoharan, A.K., Chinnathambi, S., Jayavel, R. and Hanagata, N. (2017) 'Simplified detection of the hybridized DNA using a graphene field effect transistor', *Sci. Technol. Adv. Mater.*, Vol. 18, No. 1, pp.43–50.

Monga, U., Borli, H. and Fjeldly, A. (2010) 'Compact subthreshold current and capacitance modelling of short-channel double-gate MOSFETs', *Mathematical and Computer Modelling*, Vol. 51, Nos. 7–8, pp.901–907.

Song, S.M., Bong, J.H., Hwang, W.S. and Cho, B.J. (2016) 'Improved drain current saturation and voltage gain in grapheme-on-silicon field effect transistors', *Scientific Reports*, Vol. 6, No. 25392, pp.1–8.

Svensson, J. and Campbell, E.E.B. (2011) 'Schottky barriers in carbon nanotube-metal contacts', *Journal of Applied Physics*, Vol. 110, No. 11, pp.1010–1366.

Uysal, S.O.K. and Tanoglu, G. (2017) 'An efficient iterative algorithm for solving non-linear oscillation problems', *Filomat*, Vol. 31, No. 9, pp.2713–2726.

Varghese, S.S., Varghese, S.H., Swaminathan, S., Singh, K.K. and Mittal, V. (2015) 'Two-dimensional materials for sensing: graphene and beyond', *Electronics*, Vol. 4, No. 3, pp.651–687.

Viswanathan, S., Narayanan, T.N., Aran, K., Fink, K.D., Paredes, J., Ajayan, P.M., Filipek, S., Miszta, P., Tekin, H.C., Inci, F., Demirci, U., Li, P., Bolotin, K.I., Liepmann, D. and Renugopalakrishanan, V. (2015) 'Graphene-protein field effect biosensors: glucose sensing', *Materials Today*, Vol. 18, No. 9, pp.513–522.

Xie, D. (2017) 'New finite element iterative methods for solving a nonuniform ionic size modified Poisson-Boltzmann equation', *International Journal of Numerical Analysis and Modelling*, Vol. 14, Nos. 4–5, pp.688–711.